Framework for assessing lateral flows and fluxes during floods in a conduit-flow dominated karst system using an inverse diffusive model

Cybèle Cholet[1,2], Jean-Baptiste Charlier[2], Roger Moussa[3], Marc Steinmann[1], and Sophie Denimal[1]

[1]Chrono-Environment, UMR 6249 UBFC/CNRS, University of Burgundy Franche-Comté, Besançon, 25000, France
[2]BRGM, 1039 rue de Pinville, F-34000 Montpellier, France
[3]INRA, UMR LISAH, 2 Place Pierre Viala, F-34060 Montpellier, France

Correspondence to: Cholet Cybèle (cybele.cholet@univ-fcomte.fr)

Abstract. The aim of this study is to present a framework giving new keys to characterize the spatio-temporal variability of lateral exchanges for flows and fluxes in a karst conduit network during flood events. An inverse model using an analytical solution of the diffusive wave model is applied on data from two successive gauging stations to simulate exchange dynamics after recharge. The study site is the karst conduit network of the Fourbanne aquifer in the French Jura Mountains, which includes two reaches of 5-10 km characterizing the network from sinkhole to cave stream, and to the spring. The model is applied after separation of the base and the flood components on discharge and total dissolved solids (TDS) in order to assess lateral flows and mass-fluxes and compare them to help identify water origin. Our results showed various lateral contributions in space - between the two reaches located in the unsaturated (R1), and in both unsaturated and saturated zone (R2) - as well as in time, according to hydrological conditions. Globally, the two reaches show a distinct response to flood routing, with important lateral inflows on R1 and large outflows on R2. By combining these results with mass flux exchanges and the analysis of flood routing parameters distribution, we showed that lateral inflows on R1 are the addition of diffuse infiltration (observed whatever the hydrological conditions) and localized infiltration in the secondary conduit network (tributaries) in the unsaturated zone, except in extreme dry periods. On R2, despite inflows on the base component, lateral outflows are observed during floods. This pattern was attributed to the concept of reversal flows of conduit/matrix exchanges, inducing a complex water mixing effect in the saturated zone. From our results we build the functional scheme of the karst system. It demonstrates the impact of the saturated zone on matrix/conduit exchanges in this shallow phreatic aquifer, and highlights the important role of the unsaturated zone on storage and transfer functions of the system.

1 Introduction

Hydraulic transfers and solute transport processes in karst aquifers are known very complex due to the organization of underground void structures leading to preferential drainage axis through a conduit network embedded in a less permeable fissured matrix (Kiraly, 2003; Ford and Williams, 2013). Flow processes are driven by the spatial variability of the geometrical elements that constitute the conduit network as full pipes, open channels, or pipe constrictions (Covington et al., 2009), leading

to rapid evolving the transitions from free-surface to pressurized flows, after recharge events. In such heterogeneous media, transport parameters are also dependent on scale effect, as mentioned by (Hauns et al., 2001) who showed that retardation factor is dominant at a local scale but subside for the benefit of an increase in dispersivity with distance. In addition to the interaction between conduit and matrix compartments (Martin and Dean, 2001), concentration evolutions in the conduit network

5   are strongly influenced by the mixing with inflows from tributaries (Perrin et al., 2007) or with flooded areas (Dewaide et al., 2016). These last papers pointed out the various and complex lateral exchanges along the conduit network, which remains an open question calling for new tools to investigate it.

Natural and artificial tracers are commonly used in catchment hydrology to better understand the spatial variability of lateral

10   exchanges in order to study flows and fluxes between main channel and adjacent hydrological units. Ruehl et al. (2006) highlighted strong channel losses despite storage exchange fluxes and lateral inflows. By analysing exchanges between consecutive reaches in a mountainous headwater stream, Payn et al. (2009) emphasized the importance of the geomorphological context as a driver for the spatial variability of gaining and losing reaches. Moreover, they demonstrated that many of the studied reaches were concurrently losing and gaining. Szeftel et al. (2011) simulated mass-flux exchanges using the OTIS model (Runkel and

15   Chapra, 1993; Runkel, 1998), which is a 1-D finite-difference model solving solute transport in the streams accounting for transient storage. By testing the influence of different conceptualizations of hydrologic exchanges on the estimation of transient storage parameters, they showed the complexity to model tracer evolution, due to the difficulty to quantify spatial patterns and magnitudes of lateral inflows and outflows. The same model was recently used by Dewaide et al. (2016) to simulate lateral exchanges in karst conduits in both unsaturated ("river stretches") and saturated zone ("flooded area"). This study furthermore

20   showed that the parametrization of solute transport in the system was strongly impacted by interactions within the saturated zone. However, all these works were designed for low flow periods and are therefore not suitable to investigate the temporal evolution of lateral flows during flood events in conduit-flow dominated karst systems with large quick flows.

To assess hydrodynamic processes, Saint-Venant equations (SVE) describe unsteady flow in partially filled conduits (Saint-

25   Venant, 1871) and are generally used to simulate discharge in conduit-flow dominated karst aquifers. As the conduit flow in the unsaturated zone is mainly controlled by free-surface conditions, Manning's equations are favoured, although they underestimate head losses due to turbulent flows (Jeannin and Marechal, 1995). Equations to be used for the saturated zone should be adapted for pressurized conditions, such as the Preissmann slot model in ModBraC (Reimann et al., 2011), or the Darcy-Weisbach equation in pipe-flow models like the Storm Water Management Model (SWMM) (Jeannin, 2001; Campbell and

30   Sullivan, 2002; Peterson and Wicks, 2006; Chen and Goldscheider, 2014). However, application of these models is questionnable, because detailed informations– often not available - on hydraulic parameters are required, particularly concerning the location and geometry of conduits. As a consequence, such physically-based models are often applied in a degraded mode (Le Moine et al., 2008), and are sometimes over-parameterized even in case of relatively well-known conduit networks. An alternative approach to model hydraulic processes would be to test the ability of simplified SVE with parsimonious parameters.

35   For that, following Moussa and Bocquillon (1996b), the diffusive wave equation can be considered as a simplification of the

full SVE, and is even a higher order approximation than the uniform formulae (i.e. Manning's formula). This approach was used successfully by Charlier et al. (2015) to assess lateral flows in karst rivers with numerous lateral in- and outflows. It is therefore a promising alternative to the more complex approaches cited above.

5   One of the methods used to simplify the SVE, which consists of the continuity equation and the momentum equation, is the diffusion-wave method (DW) that neglects the acceleration terms (Moussa and Bocquillon, 1996b). Combined with Manning's equation or Chezy's equation, the DW equations can be simplified to one single equation (Moussa, 1996; Fan and Li, 2006; Wang et al., 2014). This equation can be applied to a wide range of phenomena in different fields as exposed by Singh (2002) for the kinematic wave. In fact, DW is largely used for flood routing model but also for solute transport, known as
10 the advection-diffusion model (Cimorelli et al., 2014). With the assumption of constant values for wave celerity and diffusion coefficient (Hayami (1951) hypothesis) and in the particular case of uniformly distributed lateral flow, an analytical solution unconditionally stable of the Hayami model exists Moussa (1996). The inverse model needs as input the inflow hydrograph, the outflow hydrograph and a predetermination of the celerity and diffusivity; the inverse model enables to identify the temporal distribution of the lateral flow which can be either positive (lateral inflow) or negative (lateral outflow). The applied direct and
15 inverse model of this analytical solution belong to the hydrological model MHYDAS (Distributed Hydrological Modelling of AgroSystems) and was described in Moussa et al. (2002). By using the inverse model, it is possible to simulate lateral inflows or outflows between two gauging stations during a flood event and to identify more accurately exchanges from lateral hydrogeological units along the main conduit of a karst system.

20 To model conservative solute transport along a 1D flow path, the advection-dispersion equation (ADE) is largely used in hydrology (Runkel, 1996; Baeumer et al., 2001) and karst hydrology (Hauns et al., 2001; Luhmann et al., 2012). Under steady-state flow conditions, and in agreement with the mass conservation law, solute mass fluxes can be expressed by ADE. However, ADE is more challenging to implement in case of unsteady-state flow conditions, especially when lateral exchanges occur.

In the present study, following (Singh, 2002), the diffusive wave model was applied for flux transfer, the flux being either
25 discharge or mass flux. Under the hypothesis of uniformly distributed lateral fluxes, the analytical Hayami solution and the corresponding inverse model proposed by (Moussa, 1996) were used. Thereby, we present a new framework combining the diffusive wave model not only as a flood routing model, but also as a transfer function for mass propagation. Inverse modelling is used to identify lateral flows and estimate their concentrations coupling both, water flow and mass fluxes. The framework is tested on discharge and total dissolved solids data from two reaches of a karst conduit for several flood events under various
30 hydrological conditions, with the aim to characterize lateral variability of flow and mass-flux exchanges.

2 Modelling approach

2.1 Assessing lateral flows

2.1.1 Diffusive wave model without lateral flows

The diffusive wave equation is an approximation of the Saint-Venant equations used to model 1D unsteady flow in open
5 channels (Moussa and Bocquillon, 1996b):

$$\frac{\partial Q}{\partial t} + C_Q \frac{\partial Q}{\partial x} - D_Q \frac{\partial^2 Q}{\partial x^2} = 0 \tag{1}$$

where x [L] is the length unit, t [T] is the time, moreover the celerity C_Q [LT^{-1}] and the diffusivity D_Q [L^{2}T^{-1}] are functions
of the discharge Q [L^{3}T^{-1}].

Between two stations I (inflow) and O (outflow), the model is applied on the flood component ($Q_{I,flood}(t)$ and $Q_{O,flood}(t)$) of
10 the total discharge ($Q_{I,tot}(t)$ and $Q_{O,tot}(t)$), which can be deduced from an hydrograph separation by removing the baseflow
components $Q_{I,base}(t)$ and $Q_{O,base}(t)$:

$$Q_{I,flood}(t) = Q_{I,tot}(t) - Q_{I,base}(t) \tag{2}$$

$$Q_{O,flood}(t) = Q_{O,tot}(t) - Q_{O,base}(t) \tag{3}$$

Based on the Hayami assumptions (Hayami, 1951), considering C_Q and D_Q as constant parameters over time along a channel
15 network of length L, and without downstream boundary condition, the direct model of the diffusive wave equation without
lateral exchange can be written as follows (Moussa, 1996):

$$Q_{I,routed}(t) = Q_{I,flood}(t) * K_Q(t) \tag{4}$$

The symbol $*$ representing the mathematical convolution function and the Hayami kernel function $K_Q(t)$, which is expressed
as follows:

20 $$K_Q(t) = \frac{L}{2(\pi D_Q)^{1/2}} \frac{exp[\frac{C_Q L}{4 D_Q}(2 - \frac{L}{C_Q t} - \frac{C_Q t}{L})]}{(t)^{3/2}} \tag{5}$$

A first estimation of C_Q and D_Q can then be obtained comparing $Q_{I,routed}(t)$ to $Q_{O,flood}(t)$.

2.1.2 Diffusive wave model with lateral flows

By considering the existence of lateral flow exchanges along a channel reach, we obtain (Moussa et al, 1996):

$$\frac{\partial Q}{\partial t} + C_Q(\frac{\partial Q}{\partial x} - q) - D_Q(\frac{\partial^2 Q}{\partial x^2} - \frac{\partial q}{\partial x}) = 0 \tag{6}$$

25 where $q(x,t)$ [L^2.T^{-1}] is the lateral flow rate per unit length as a function of distance along the channel reach x. The expression
$q(x,t)$ may be positive or negative depending on the occurrence of lateral inflow or outflow, respectively (Fig. 1).

An analytical resolution of the diffusive wave equation with lateral flows is proposed by Moussa (1996) based on the Hayami assumptions, accounting for uniformly distributed lateral flow between two gauging stations I (inflow) and O (outflow).

$$Q_{I,routed}(t) = \Phi_Q(t) + (Q_{I,flood}(t) - \Phi_Q(t)) * K_Q(t) \tag{7}$$

$$\text{with} \quad \Phi_Q(t) = \frac{C_Q}{L} \int_0^t (Q_{A,flood}(\lambda) - Q_{A,flood}(0))d\lambda \tag{8}$$

where $d\lambda$ is the variable along which the integral function is calculated.

The lateral flood flows $Q_{A,flood}(t)$ along the reach, under the hypothesis of uniformly distributed lateral flow, is expressed as:

$$Q_{A,flood}(t) = \int_0^t q(x,t)dx \tag{9}$$

The inverse model enables the identification of the temporal distribution of the lateral inflows or outflows $q(x,t)$ over the channel reach. According to Moussa (1996), by knowing $Q_{I,flood}(t)$ and $Q_{O,flood}(t)$, it is possible to calculate $Q_{A,flood}(t)$. Eq. 7 gives then:

$$A_Q(t) = Q_{O,flood}(t) - Q_{I,flood}(t) * K_Q(t) \tag{10}$$

$$\text{with} \quad \Phi_Q(t) - \Phi_Q(t) * K_Q(t) = A_Q(t) \tag{11}$$

The resolution of equations (10) and (11) requires first the identification of $K_Q(t)$ using equation (5), and consequently a predetermination of the two parameters C_Q and D_Q, to calculate afterwards lateral flow $Q_A(t)$ as follows:

$$Q_{A,tot}(t) = Q_{A,base}(t) + Q_{A,flood}(t) \tag{12}$$

$$\text{with} \quad Q_{A,flood}(t) = \frac{L}{C_Q} \frac{d\Phi_Q}{dt} \tag{13}$$

$$\text{and} \quad Q_{A,base}(t) = Q_{O,base}(t) - Q_{I,base}(t) \tag{14}$$

2.2 Assessing lateral mass fluxes

Classical 1D advection-dispersion equation (ADE) for steady-state flow conditions is analogous to the DW equation (Eq. 1), replacing discharge by solute concentration, and celerity and diffusivity parameters by advective velocity and dispersion parameters, respectively. In unsteady-state flow conditions, and when lateral fluxes occurred, the application of ADE is not so obvious. We propose here to assess lateral mass fluxes (defined by Eq. 15) during flood, applying the DW model accounting for lateral exchanges, as a transfer function. We assume in that case that the mass conservation law is maintained and is equivalent to the volume conservation law in the diffusive wave model. Thus, the analytical solution of Moussa (1996) is used to resolve the conservative solute mass transfer accounting for uniformly distributed lateral fluxes.

$$M(t) = S(t).Q(t) \tag{15}$$

where $M(t)$ is the solute mass flux $[\mathrm{MT}^{-1}]$, $S(t)$ is the solute concentration $[\mathrm{ML}^{-3}]$ and $Q(t)$ is the discharge $[\mathrm{L}^3\mathrm{T}^{-1}]$

As previously described for water flows, the model involves first the determination of the flood ($M_{I,flood}(t)$ and $M_{O,flood}(t)$) and base ($M_{I,base}(t)$ and $M_{O,base}(t)$) components of the total fluxes ($M_{I,tot}(t)$ and $M_{O,tot}(t)$) based on mass-chemograph separation:

$$M_{I,flood}(t) = M_{I,tot}(t) - M_{I,base}(t) \tag{16}$$

$$M_{O,flood}(t) = M_{O,tot}(t) - M_{O,base}(t) \tag{17}$$

Then, following the method described above for water flows, lateral solute mass exchange $M_A(t)$ is calculated by adapting Eqs. 5, 7, 10 and 11 as follows:

$$M_{O,flood}(t) = \Phi_M(t) + (M_{I,flood}(t) - \Phi_M(t)) * K_M(t) \tag{18}$$

$$\text{with} \quad \Phi_M(t) = \frac{C_M}{L} \int_0^t (M_{A,flood}(\lambda) - M_{A,flood}(0))d\lambda \tag{19}$$

The kernel function for the solute mass flux, $K_M(t)$, is expressed as:

$$K_M(t) = \frac{L}{2(\pi D_M)^{1/2}} \frac{exp[\frac{C_M L}{4 D_M}(2 - \frac{L}{C_M t} - \frac{C_M t}{L})]}{(t)^{3/2}} \tag{20}$$

Finally, this modelling framework combining the calculation of both lateral water flows $Q_A(t)$ and solute mass fluxes $M_A(t)$, allows the assessment of the solute concentration of the lateral flows $S_A(t)$ in the case of positive or negative $Q_A(t)$ and $M_A(t)$:

$$S_A(t) = \frac{M_A(t)}{Q_A(t)} \tag{21}$$

2.3 Framework

We propose in this section a step by step structure to help readers using our framework to investigate the exchange dynamics of water flows and conservative solute mass fluxes along a channel reach between two gauging stations. To simulate lateral exchange flows Q_A and fluxes M_A during floods, required data are discharge and solute time series from both stations covering a complete flood event. The inverse modelling of the lateral flood component include four parameters corresponding to C_Q and D_Q for water flow and C_M and D_M for mass fluxes. A graphic representation of this framework is given in Fig. 2:

(1) Collection of discharge ($Q_{I,tot}$ & $Q_{O,tot}$) and concentration ($S_{I,tot}$ & $S_{O,tot}$) data from input and output stations.

(2) Calculation of the total mass fluxes $M_{I,tot}$ and $M_{O,tot}$ using Eq. (15).

(3) Determination of the base and flood components by hydrograph ($Q_{I,tot}$, $Q_{O,tot}$) separation defined by Eqs. (2) & (3) and mass-chemograph ($M_{I,tot}$ and $M_{O,tot}$) separation defined by Eqs (16) & (17). The base and flood components are separated with the constant slope method (McCuen, 2004) by using the inflection point on the hydrograph recession. The inflection point determined on the hydrograph is used to separate base and flood components for both hydrograph and mass-chemograph.

(4) Calculation of the lateral base component for water flow ($Q_{A,base}(t)$) and mass fluxes ($M_{A,base}(t)$), using Eq. (14).

(5) Modelling of the lateral flood exchanges, using:

A. first, the direct model (Eq. (4)) to parametrize C_Q & D_Q and C_M & D_M with a trial-and-error optimization, calculating $Q_{I,routed}$ and $M_{I,routed}$ to get the best fit with $Q_{O,flood}$ and $M_{O,flood}$, respectively. The model is parsimonious with only the two parameters (celerity and diffusivity) to optimize. These two parameters are independent, hence the parametrization procedure using a trial-and-error optimization give similar results than a automatic optimization and converge rapidly to a unique and a stable solution. Nevertheless, if the user need to optimize more parameters, an automatic optimization procedure is necessary.

B. Afterwards, the inverse model is applied to simulate lateral flood exchanges $Q_{A,flood}(t)$ and $M_{A,flood}(t)$, using Eqs. (10), (11) & (13).

(6) Simulation of the total lateral exchanges $Q_{A,tot}(t)$ and $M_{A,tot}(t)$, using Eq. (12).

(7) Calculation using Eq. (21) of the solute concentrations of lateral base and flood flows $S_{A,base}(t)$ and $S_{A,flood}(t)$, respectively. And determination, if possible, of the total solute concentration $S_{A,tot}(t)$.

In our study, the application of this framework is done separately on various selected flood event. Hence, the two parameters set (C_Q & D_Q and C_M & D_M) are calibrated for each event. Then, the relationships between the parameters and the variations of water flow and mass flux are analysed. It can be expected for example that C_Q & D_Q should increase with a floodpeak increase. Finally, the compilation of all results lead us to define a functional scheme of the studied karst system.

3 Study site

3.1 Field situation

The study site is located in the Doubs river valley at the northern limit of the Jura Mountains in Eastern France, near the village of Fourbanne ($47°19'54"N6°18'15"E$, Fig 3a). The Fourbanne site is one of the experimental sites of the "Jurassic Karst" hydrogeological observatory ($http://zaaj.univ-fcomte.fr/spip.php?article13$) and monitored continuously since December 2013. The local geological structure is characterized by tabular Jurassic limestones and shales, crosscut by N-S trending normal faults (Charmoille, 2005). The recharge area of the site covers about 30 km^2. The site was selected for

its dominantly allogenic recharge and its well-developed, partially accessible conduit network. The upstream recharge area corresponds to a surface watershed underlain by impervious lower Jurassic marls. The conduit network is fed by swallow holes located at normal faults, bringing into contact lower Jurassic shales and karstified middle Jurassic limestones (Fig. 3b). The Verne swallow hole constitutes the main infiltration point of the Fourbanne karst system and corresponds to monitoring station

5   s1. The allochtonous recharge joins the well-developed cave stream of the "En-Versennes" cave, which is completely explored over a distance of about 8 km. An artificial well near the village of Fontenotte gives direct access to the cave stream, where monitoring station s2 was installed, about 5 km downstream of station s1. The Fontenotte cave stream can be followed for another 2 km downstream of station s2, where it disappears into an inaccessible conduit network. It joins finally the Fourbanne spring, which is fed by a saturated siphon of 25 m depth and explored by cave-divers over the last 500 m. Monitoring station

10   s3 was installed at the Fourbanne spring.

The climate is temperate with both oceanic and mountainous influence. Rainfall averages 1200 mm/year, occurring mainly in autumn and winter, but with slightly higher intensities in summer (Vermot-Desroches, 2015). Based on long-term records in the Jura Mountains, the number of rainy days per year is 140 on average (Charlier et al., 2012), corresponding for the most part to low-intensity rainfall events: 50% of rainy days had less than 3 mm of rainfall, whereas days between 15 and 30 mm of

15   rainfall represented only 10% of rainy days.

3.2   Field monitoring and data processing

Discharge (Q) and electrical conductivity (EC) were monitored continuously at 15 minute intervals from January to June 2015 at the three stations (Fig. 3b): the Verne swallow hole (station s1), the Fontenotte cave stream (station s2,) and the Fourbanne spring (station s3). Stations s1 and s2 were equipped with OTT CTD probes for conductivity, temperature, and

20   water level monitoring, whereas a OTT-Hydrolab DS5X multiparameter probe was used at station s3 for conductivity and water temperature, and a OTT Orpheus mini probe for water level. The three stations divided the main conduit into two reaches: R1 from s1 to s2 (3.1 km) and R2 from s2 to s3 (5.4 km, Fig 3c). Hourly precipitation were recorded by a fully automatic Campbell BWS200 weather station installed next to monitoring station s2 in the Fontenotte village.

From the available time series, 7 flood events with complete data sets for all stations and various rainfall intensities were

25   selected. A synthetic characterization of the 7 events is given in Fig. 4, where they are sorted from event 1 to 7 in function of decreasing baseflow at system outlet (station s3). The event duration varied from 24 to 52 hours with total precipitation amounts between 3.4 to 46.6 mm. A progressive decrease of the hydrogeological response with decreasing baseflow was found for events 1 to 5, whereas events 6 and 7 from an extremely dry period in June 2015 behaved differently with an important inflow from the station s1.

30   The EC is directly related to the Total Dissolved Solids (TDS) assuming that TDS represent mainly conductive ionic compounds. The TDS values were therefore calculated directly from EC by using a constant factor of 0.64 (100 S.cm^{-1} = 64 g.l^{-1}), which is commonly used by OTT CTD probes and consistent with the literature (Lloyd and Heathcote, 1985) according to the water mineralization range of the data set.

3.3 Model application to the study site

To illustrate the model behaviour described theoretically in Section 2 and to help to define a parametrization strategy, this section presents a sensitivity analysis on a representative event. We assume that the analysis carried out on a benchmark flood event is representative of the model parameters sensitivity on the other events.

3.3.1 Sensitivity analyses

This analysis was carried out on the celerity C_Q and the diffusivity D_Q for the direct and the inverse model, both applied on water flows. The celerity C_Q and the diffusivity D_Q describe the propagation and the flattening of the flood peak, respectively. The model applied on fluxes using C_M & D_M is assumed to show an identical behaviour.

Figs. 5a-a' represent the routed input hydrograph and the simulated lateral flow, respectively, varying C_Q from 0.1 to 0.3 m.s^{-1} with a fixed D_Q of 0.1 m^2.s^{-1} (i.e. low D_Q value). Similarly, Figs. 5b-b' represent the same graphs, but with a fixed C_Q of 0.15 m.s^{-1} (i.e. low C_Q value) and varying D_Q from 0.1 to 10 m^2.s^{-1}.

Figs. 5a-b illustrate the application of the direct model simulating the propagation of the input signal in order to fit the output signal with the two parameters set (C_Q & D_Q) by considering no lateral exchange. The graphs clearly demonstrate that the routed input signal is much more sensitive to celerity than diffusivity. Varying C_Q by a factor of 3 has a stronger impact on the results than varying D_Q by a factor of 100. As an example, a 10% variation of C_Q (with constant D_Q) modifies the maximum of $Q_{I,flood} * K_Q$ of 9%, while 10% variation of D_Q (with constant C_Q) changes to vary the maximum of $Q_{I,flood} * K_Q$ of 0.6% only. Moreover, this sensitivity test illustrates the impact of both parameters on the propagation velocity and the shape of the flood peaks: increasing C_Q values yield more rapidly propagating and higher flood peaks, whereas increasing D_Q values lead to flattened peaks. These observations are in agreement with the literature (Moussa and Bocquillon, 1996b; Yu et al., 2000; Chahinian et al., 2006; Charlier et al., 2009) and confirm that the lower C_Q and the higher D_Q, the lower are the peak flow intensity and the transfer velocity. Figs. 5a'-b' illustrate the simulation of lateral flows using the inverse model knowing input and output signals. It shows that C_Q and D_Q influence the lateral flow rates as well as the exchange direction (inflows or outflows) which could be inversed during a same flood event. Low C_Q and D_Q values lead to lateral inflows followed by outflows, whereas high C_Q and D_Q values lead to outflows followed by inflows.

3.3.2 Parametrization strategy

From the sensitivity analysis, a parametrization strategy was defined for the application of the direct model for the four parameters: C_Q and D_Q for discharge, and C_M and D_M for the mass fluxes. The parameters were optimized by the trial-and-error method based on simulations of the routed input signals and by using the following criteria: i) C was determined first from the peak delay between two succeeding gauging stations (celerity = reach length / delay), ii), whereas D was adjusted in order to get a best fit of the shape of the hydrograph or mass-chemograph with the observed output signal.

4 Results

4.1 Simulation of lateral exchanges

Figure 6 illustrates the application of the framework (depicted in Fig. 2) for reaches R1 and R2 of the study site for flood event no. 1 with 21 mm of rainfall during high flow conditions.

5   The lateral base exchanges calculated for reach R1 demonstrate that the output signal observed at station s2 for discharge and mass flux cannot be entirely explained by the contribution of the input signal, but that it was essentially derived from lateral inflows between s1 and s2. The mass flux model shows in addition that the lateral inflows were strongly mineralized, with higher TDS values than for stations s1 and s2. The mass fluxes of the base component at station S2 were thus essentially derived from lateral inflows along reach 1. This pattern was different for reach R2, where lateral base inflows were 2-fold

10   lower and with similar TDS values. Regarding the flood components, the simulated lateral exchange indicates important lateral inflow and high mass influx along R1. The concentration estimations indicate a similar evolution than for station s2, which is characterized by a TDS dilution during the flood. In contrast, the dynamic was totally different along R2, where outflows are simulated. The concentration estimations of the lateral component deduced from outflows and mass outfluxes are very low compared to the measurements at stations s2 and s3, suggesting the presence of more complex processes than simple outflows,

15   as will be discussed later on in Section 5.2.

4.2 Variability of lateral exchanges

Following the example detailed for flood event no. 1 in the previous section, this section aims at summarizing results of the model application on all selected flood events in order to get informations on the general hydrological functioning of the field site.

20   #### 4.2.1 Lateral exchanges for the base component

Figures 7a-c present lateral exchanges for base water flow and base mass fluxes for all events of reaches R1 (orange labels) and R2 (purple labels). When comparing the modelled mean lateral base flow exchange in function of the measured mean base input, two distinct linear relationships can be observed (Fig. 7a). For both reaches, lateral exchanges were positive, indicating inflows that increased linearly with average base input. For reach R1, lateral water inflow was 2.6 fold higher than mean input

25   flow from station s1, whereas for reach R2 the mean lateral water inflow represented only 0.4 times the mean inflow from station s2. For mass fluxes (Fig. 7c) a very similar relationship was found. However, for R1 the slope of the correlation was much steeper than for water flow (4.3 against 2.6), indicating that the lateral inflow water was more mineralized than the input flow from station s1 already present in the system. In contrast, for reach R2 a lower slope was found for mass flux than for water flow (0.3 against 0.4), meaning that lateral inflow was less mineralized than input flow from station s2.

4.2.2 Lateral exchanges for the flood component

Figs. 7b-d illustrate lateral water flows and mass fluxes calculated for flood flow. To summarize the dynamics of the lateral exchanges during the flood, minimum and maximum values are presented rather than average values in order to characterize intensities of both lateral gains and losses which may occur during the same event. Along reach R1, two distinct groups are observed depending on peakflow from input station s1 (Fig. 7b): (i) Events 1 to 5 with low input values are characterized by lateral inflows, with high maxima and minima close to zero. (ii) Events 6 and 7 with high input values from strong rain events during an extremely dry period, show with maxima close to zero and strongly negative minima indicating important lateral losses. Comparing the slopes of the linear relationships for water flows (Fig. 7b) and mass fluxes (Fig. 7d), it appears that the water inputs of the first group were strongly mineralized, whereas the water losses of the second group were characterized by low mineralization. For reach R2, all maxima of water flow and mass flux are close to zero, whereas the minima are negatively correlated with input values, indicating increasing lateral losses with increasing peakflow. Comparing the slopes between water flood flow (fig 7b) and mass flood flux (fig 7d), it appears that lateral losses were systematically less mineralized than input water from station s2.

4.3 Transport dynamics towards the conduit network

4.3.1 Distribution of model parameters

In this Section we present the distribution of the model parameters - celerity and diffusivity - in function of maximum input flood flow intensities, because these data furnish information on transport dynamics (Fig. 8).

The C_Q water flow celerity parameter increased linearly with input peakflow for events 1 to 5 for reaches R1 and R2 (Fig. 8a, graph in semi-log scale). Reach R1, entirely located in the unsaturated zone, showed lower celerities compared to reach R2, which was localized in both unsaturated and saturated zone. Events 6 and 7, corresponding to the extreme dry period, did not fit this trend for both reaches, and were characterized by lower C_Q values. This behaviour may be related to the low degree of water saturation of the system at the beginning of the flood. The C_M mass flux celerity parameter showed similarly a relationship with the flood flow intensities for events 1 to 5, but only for reach R1 and again with a different behaviour for events 6 and 7 (Fig 8c). On the contrary, we did not found any relationships for reach R2, suggesting a more complex behaviour for this part of the system, most probably related to the presence of the saturated zone. All events from reaches R1 and R2 had very low D_Q diffusivities. Only events 1-4 on reach R2 showed increasing D_Q values with increasing input peakflow (Fig 8b). We note that these 4 data points were all from a wet period and from reach R2, which localized in the non-saturated and the saturated zone. The D_M mass flux diffusivity parameter showed a very similar distribution as D_Q, i.e. again with the only elevated values for events 1-4 on reach R2 (Fig 8d).

4.3.2 Assessment of the saturated level of the conduit network

The analysis of the parameter distributions showed distinct patterns for R1 and R2, which can be attributed to the presence of the saturated zone in the lower parts of reach R2 (see Figure 3 for hydrogeological scheme of the main conduit). In fact, flood routing in the unsaturated zone is related to flow in open conduits, whereas in the saturated zone it is controlled by pressure

5 transfer leading to an almost instantaneous propagation. Consequently, the difference of flood routing between unsaturated and saturated conduits along the system should be observed in the C_Q parametrization of the 2 reaches R1 and R2. In fact, by considering a mean constant slope of the main karst conduit, we hypothesize a constant C_Q value along the unsaturated zone in R1 and R2. The relation between C_Q values of R1 and R2 for each event should therefore furnish information on the localization of the limit between the saturated and the unsaturated zone. Based on these hypotheses, the Eq.(22) is used to

10 estimate the percentage of conduit length of reach R2 located within the unsaturated zone, defined as "U" value.

$$U = \frac{C_Q(R1)}{C_Q(R2)} \cdot 100 \qquad (22)$$

This limit is supposed to fluctuate in function of the baseflow condition. Figure 9a represents the U values of all events in function of the mean baseflow at the system outlet in station s3 (Fourbanne spring). A linear relationship is observed for events 1 to 6 showing - as expected - an increasing U with a decreasing mean baseflow, which is coherent with the saturation

15 level of the system measured by discharge. With an estimated total length of 5.4 km for R2, the saturated conduit length is approximatively 1.5 to 2.2 km. Event 7 shows that the system behaved differently for flood events during extreme dry periods. This point will be discussed in the next Section.

5 Discussion and conclusion

5.1 Modelling framework

20 Our study intends to present a new framework to quantify the temporal evolution of lateral flows and fluxes during floods in a well-developed karst conduit networks. It uses the diffusive wave (DW) model, which is a physically-based approach, parsimonious and easy-to-use. We used the model with an inverse approach allowing simulations of both lateral flows and mass fluxes under unsteady-state conditions following the assumption of uniformly distributed lateral exchanges.

Previous modelling studies focusing on the quantification of lateral exchanges in karst aquifers were conducted during base

25 flow at steady-state flow conditions (Dewaide et al., 2016). In contrast, the framework of the present study furnishes new keys to identify such exchanges during flood events. It allows furthermore to quantify them, to estimate their concentration, and to characterize their origin(e.g. strongly mineralized lateral inflows from the rock matrix). An important advantage of the DW model over other approaches is its a parsimonious parametrization using only two parameters (celerity C and diffusivity D) for both flow and mass fluxes processes. The Hayami model also offers an unconditionally stable method with very low computing

30 time, unlike numerical methods inducing numerical instabilities (Moussa and Bocquillon, 1996a, b). Finally, the short time-

step analysis of the results show that the modelling framework may be used as a diagnostic tool to investigate the dynamics of lateral exchanges from flood analysis.

Regarding parametrization, the analysis of the distribution of water flow parameters (celerity C_Q and diffusivity D_Q) of 7 flood events allowed to characterize the variability of flood routing variability in more detail for the reach R1 located in the

5   unsaturated zone and the reach R2 covering both unsaturated and saturated zones. Both reaches showed linearly increasing C_Q values with increasing flood intensities (Section 4.3.1.). The difference of C_Q parametrization between the two reaches was then used in Section 4.3.2 to quantify the fluctuation of the unsaturated/saturated boundary within the karst conduit. Mass flux parameters (C_M and D_M) are less obvious to interpret. Reach R1 showed a linear relationship of C_M in function of mass flux intensity, whereas a comparable trend was absent for reach R2 attesting the difficulty to characterize transport processes within

10   the saturated conduit network from the available monitoring design.

The proposed framework requires to decompose the base and the flood components, being consistent with the duality of flow processes dynamics. As proposed by many authors (Atkinson, 1977, among others), the base component typifies slow flow in the system, which is strongly influenced by interaction with the rock matrix (or low permeable volumes) with high storage capacities, whereas the flood component typifies quick flow within the conduit network with low storage capacities, which

15   is strongly linked with flood intensity. Thus, considering that baseflow is used to estimate base exchanges and the diffusive wave flood routing model to assess flood exchanges, our framework gives a deconvolution of the two components of the lateral exchanges helping to interpret the involved processes.

Our methodology quantifies total lateral water flow and mass flux exchange for a given reach, but does not allow to identify simultaneously occurring local lateral flows and fluxes as already highlighted by several authors (Payn et al., 2009; Szeftel

20   et al., 2011; Charlier et al., 2015). The results for the reach R2 furthermore denote the difficulty to decompose exchanges that occurred in part in the unsaturated and in part in the saturated zone. Lateral flood outflows for R2 were mainly combined with low flood outfluxes with total mineralisations lower than those observed for the input and output stations. This may be the result of complex exchanges occurring between conduit and matrix (or low permeable volume) water within the saturated zone, with out- and inflows occurring concomitantly during the same flood and having contrasted concentrations. The DW model thus

25   furnishes numerous information about lateral exchanges in karst aquifers. Its limitation is that it considers a reach of a conduit system as a "homogeneous" unit with uniformly distributed lateral exchanges. It is a diagnostic tool which naturally cannot be used to decipher too much complexity in the case of too remote monitoring stations with highly variable lateral contributions. As reported by Szeftel et al. (2011), we point out the limits of our framework to identify a single, unambiguous model structure representing transport processes when boundary conditions are poorly described.

30   ## 5.2   Functional scheme

The modelling framework is proposed as a diagnostic tool to assess the dynamics of lateral exchanges between the main conduit and the neighbouring compartments of the karst aquifers during floods. The model application on several contrasted events on the Fourbanne karst network gives several points of discussions to evaluate exchanges in various hydrological conditions and allow to dress a general hydrological functional scheme of the site. This scheme, presented in Fig. 10, highlights the lateral

contributions for the base and the flood components. In fact, we assume that - as discussed before - base and flood components are mainly related to specific processes as conduit/matrix exchanges distinguished by slow and fast flow, respectively.

(a) For major precipitations during high flow periods (events no. 1 and 2; fig10a) we showed the importance of lateral exchanges for both base and flood components. For the baseflow component both reaches were fed by higher mineralised lateral inflows. However, for the flood component the model yielded different results for the two reaches. Reach R1, located entirely in the unsaturated zone, obtained lateral inflows which were more mineralized than the sinking stream at the reach input. We relate these higher mineralized inputs to the arrival of tributaries from adjacent sinkholes (see their location on Fig. 3). On the contrary, reach R2 shows less mineralized base inflows and mainly slightly mineralized flood outflows, indicating high losses, which we relate to mixing processes in the saturated part of the conduit.

(b) For minor precipitations during low flow periods (events no. 3, 4 and 5; fig10b) reach R1 showed similarly mineralised inflows from the base and the flood components, but with a lower inflow amount in coherence with the lowest rainfall intensity of these events. On the contrary, the baseflow component of reach R2 was mainly characterized by inflows, whereas weak outflows were found for the flood component. This shows that the system was mainly influenced by the drainage of water from the rock matrix even during low flow periods. The weak outflows found for the flood component of reach R2 probably occurred within the saturated zone.

(c) For major precipitations during extremely dry periods (events no. 6 and 7; fig 10c) a quite different behaviour was observed. Reach R1 presented very low base inflows with similar mineralizations as for the input flow, probably derived from sinking stream tributaries joining the unsaturated conduit network. However, important outflows were observed for the flood component, indicating high losses towards the rock matrix in the unsaturated zone. On the contrary, reach R2 presented very low baseflow inputs of highly mineralized water. The flood component was characterized mainly by lateral outflows followed by lowest inflows . It is interesting to denote this reversal of the lateral flood flows from out- to inflows, indicating an evolution of the exchanges during the flood event, that we may be related to conduit/matrix interactions in the saturated zone.

Even if we observed increasing lateral inflows with increasing baseflow conditions, a slow inflow component remained always present all along the network (i.e. in the unsaturated as well as in the saturated zone), whatever the hydrological conditions (cf. section 4.2.1.). These constant inflows could probably originate mainly from diffuse infiltration in the unsaturated zone and from lateral drainage systems in the saturated zone. However, the mineralization of the infiltrating water was higher along R1 compared to R2, reflecting probably different recharge mechanisms. It seems that reach 1 collected additional inflows from strongly mineralized secondary tributaries mainly localized in the upstream part of the aquifer (R1), in accordance with the presence of sinkholes in the north-eastern part of the study area (Fig. 3).

In Section 4.2.2., from the analysis of the event's distribution according to rainfall intensity and initial baseflow we could distinguish 2 distinct groups of events depending on the general hydrological context: (1) events 1 to 5 during periods of high and low flow, and (2) events 6 & 7 from an extremely dry period. The evolution of the lateral flood exchange for group (1) increased linearly with flood intensity (maximum of the peak flood, Fig. 7), suggesting that these lateral inflows, probably

5 derived from secondary conduits, were proportional to the discharge measured at the input station. For reach R1, the mineralisation of these inflows increased with maximum input inflow, whereas for reach R2 the mineralisation of outflows decreased. For group (2), lateral flood outflows were observed along both reaches, and notably for R1, meaning that the inflows from secondary lateral conduits observed for group (1) stopped during extreme dry periods in the unsaturated zone. This change of behaviour compared to group (1) showed the non-linearity of the lateral exchanges depending on hydrological conditions. This

10 threshold effect in the hydrogeological response may be related to the presence of epiphreatic conduits (Jeannin, 2001) leading to time-variant limits of their recharge area (Jukić and Denić-Jukić, 2009; Charlier et al., 2012).

To our opinion, from the available data, two types of outflows along the karst conduit network can be described in our conceptual model. The first type corresponds to outflows observed along R1 during the extremely dry period. These outflows occurred in the unsaturated zone of the conduit at extremely low baseflow conditions where only very few base inflows were

15 observed. Thus, during this period, the flood input following major precipitations recharged the low permeability volume (or matrix) from the conduit network. The second type corresponds to outflows observed along R2 for all baseflow conditions. These outflows seemed to occur in the saturated zone and are related to flow reversal occurring in the saturated conduit as mentioned by several authors (Jeannin, 1996; Maréchal et al., 2008; Bailly-Comte et al., 2010) who demonstrated the influence of the contrasted kinetics fluctuations of the hydraulic head between the conduit and the surrounding matrix during a flood

20 event. This conduit/matrix relationship in the saturated zone probably induces a complex water mixing effect inside of karst conduit during the flood event.

Besides these results, the flood routing parameters are also indicators for hydraulic processes in the conduit. They are used in section 4.3.2. to estimate the fluctuation of the limit between the unsaturated and the saturated zone within reach R2. We evaluated that the saturated zone occupied 25% to 40% of R2, depending on flow conditions, corresponding to the 1.5 to 2.2

25 km of conduit next to the outlet station s3. The Fourbanne karst system with its total length of 8.5 km (3.1 km for R1 and 5.4 km for R2) is thus a shallow-phreatic aquifer. Consequently, we demonstrated that besides the impact of the saturated zone on the matrix/conduit exchanges, the unsaturated zone plays a major role on the flood genesis in karst aquifers. Our results confirm that the unsaturated zone has essentially a transfer function – as it is commonly conceptualized (Bakalowicz, 2005) – leading to a rapid hydrological response at the spring due to the high connectivity of the conduit networks. But in our case,

30 we denoted also that a large part of water storage (assessed by the baseflow component in the different stations) originate from this zone. This result highlighted the important storage function of the unsaturated zone as previously pointed in works using hydrochemical approaches (Emblanch et al., 2003; Mudarra and Andreo, 2011), but often minimized in current conceptual karst models.

In conclusion, we showed that the inverse modelling framework of the diffusive wave gives new keys to characterize the

35 contrasted dynamics of lateral exchanges for base and flood lateral exchanges occurring along the conduit network in both

unsaturated and saturated zone. One of the main points was the ability of our framework to propose a deconvolution of the output hydrograph as well as mass-chemograph allowing to quantify the lateral contributions in terms of flows and mineralization. Finally, as illustrated by the building of a conceptual model of the study case, our framework provided opportunities to experiment and investigate lateral flows and fluxes of karst conduit networks, known to have large amount of concomitant in-

5 and outflows.

Acknowledgements. The authors wish to thank Bruno Régent for his active contribution on the field. Many thanks to the Speleology Association of Doubs Central (ASDC) for the precious help on the field and their support to access to the Fontenotte river cave stream in the En-Versennes karst network. We thank Jacques Prost for the welcoming of our monitoring equipment and to give us access to the Fourbanne spring. We also thank the Verne municipality to let us monitoring the Verne swallow hole. This work was carried out with the financial

10 support of the Burgundi-Franche-Comté Region and the BRGM.

References

Atkinson, T.: Diffuse flow and conduit flow in limestone terrain in the Mendip Hills, Somerset (Great Britain), Journal of Hydrology, 35, 93–110, doi:10.1016/0022-1694(77)90079-8, 1977.

Baeumer, B., Benson, D. A., Meerschaert, M. M., and Wheatcraft, S. W.: Subordinated advection-dispersion equation for contaminant transport, Water Resources Research, 37, 1543–1550, 2001.

Bailly-Comte, V., Martin, J. B., Jourde, H., Screaton, E. J., Pistre, S., and Langston, A.: Water exchange and pressure transfer between conduits and matrix and their influence on hydrodynamics of two karst aquifers with sinking streams, Journal of Hydrology, 386, 55–66, doi:10.1016/j.jhydrol.2010.03.005, 2010.

Bakalowicz, M.: Karst groundwater: a challenge for new resources, Hydrogeology Journal, 13, 148–160, doi:10.1007/s10040-004-0402-9, 2005.

Campbell, C. and Sullivan, S. M.: Simulating time-varying cave flow and water levels using the Storm Water Management Model, Engineering Geology, 65, 133–139, doi:10.1016/S0013-7952(01)00120-X, 2002.

Chahinian, N., Moussa, R., Andrieux, P., and Voltz, M.: Accounting for temporal variation in soil hydrological properties when simulating surface runoff on tilled plots, Journal of Hydrology, 326, 135–152, doi:10.1016/j.jhydrol.2005.10.038, 2006.

Charlier, J.-B., Moussa, R., Cattan, P., Cabidoche, Y.-M., and Voltz, M.: Modelling runoff at the plot scale taking into account rainfall partitioning by vegetation : application to stemflow of banana (Musa spp.) plant, Hydrology and Earth System Sciences Discussions, 13, 2151–2168, 18 pages, 2009.

Charlier, J.-B., Bertrand, C., and Mudry, J.: Conceptual hydrogeological model of flow and transport of dissolved organic carbon in a small Jura karst system, Journal of Hydrology, 460–461, 52–64, doi:10.1016/j.jhydrol.2012.06.043, 2012.

Charlier, J.-B., Moussa, R., Bailly-Comte, V., Danneville, L., Desprats, J.-F., Ladouche, B., and Marchandise, A.: Use of a flood-routing model to assess lateral flows in a karstic stream: implications to the hydrogeological functioning of the Grands Causses area (Tarn River, Southern France), Environmental Earth Sciences, 74, 7605–7616, doi:10.1007/s12665-015-4704-0, 2015.

Charmoille, A.: Traçage hydrochimique des interactions hydrauliques et mécaniques entre les volumes perméables et peu perméables au sein des aquifères fracturés carbonatés - Aquifère karstique de Fourbanne (Avant-pays jurassien, 25) et Laboratoire naturel de Coaraze (Alpes Méridionales, 06), phdthesis, Université de Franche-Comté, 2005.

Chen, Z. and Goldscheider, N.: Modeling spatially and temporally varied hydraulic behavior of a folded karst system with dominant conduit drainage at catchment scale, Hochifen–Gottesacker, Alps, Journal of Hydrology, 514, 41–52, doi:10.1016/j.jhydrol.2014.04.005, 2014.

Cimorelli, L., Cozzolino, L., Della Morte, R., and Pianese, D.: Analytical solutions of the linearized parabolic wave accounting for downstream boundary condition and uniform lateral inflows, Advances in Water Resources, 63, 57–76, doi:10.1016/j.advwatres.2013.11.003, 2014.

Covington, M. D., Wicks, C. M., and Saar, M. O.: A dimensionless number describing the effects of recharge and geometry on discharge from simple karstic aquifers, Water Resour. Res., 45, W11 410, doi:10.1029/2009WR008004, 2009.

Dewaide, L., Bonniver, I., Rochez, G., and Hallet, V.: Solute transport in heterogeneous karst systems: Dimensioning and estimation of the transport parameters via multi-sampling tracer-tests modelling using the OTIS (One-dimensional Transport with Inflow and Storage) program, Journal of Hydrology, 534, 567–578, doi:10.1016/j.jhydrol.2016.01.049, 2016.

Emblanch, C., Zuppi, G., Mudry, J., Blavoux, B., and Batiot, C.: Carbon 13 of {TDIC} to quantify the role of the unsaturated zone: the example of the Vaucluse karst systems (Southeastern France), Journal of Hydrology, 279, 262 – 274, doi:10.1016/S0022-1694(03)00180-X, 2003.

Fan, P. and Li, J.: Diffusive wave solutions for open channel flows with uniform and concentrated lateral inflow, Advances in Water Resources, 29, 1000–1019, doi:10.1016/j.advwatres.2005.08.008, 2006.

Ford, D. and Williams, P. D.: Karst Hydrogeology and Geomorphology, John Wiley & Sons, google-Books-ID: whgNDVXFiqYC, 2013.

Hauns, M., Jeannin, P.-Y., and Atteia, O.: Dispersion, retardation and scale effect in tracer breakthrough curves in karst conduits, Journal of Hydrology, 241, 177–193, doi:10.1016/S0022-1694(00)00366-8, 2001.

Hayami, S.: On the propagation of flood waves., Bulletins - Disaster Prevention Research Institute, Kyoto University, pp. 1–16, 1951.

Jeannin, P.-Y.: Structure et comportement hydraulique des aquifères karstiques, Ph.D. thesis, Université de Neuchâtel - Faculté des sciences, 1996.

Jeannin, P.-Y.: Modeling flow in phreatic and epiphreatic Karst conduits in the Hölloch Cave (Muotatal, Switzerland), Water Resour. Res., 37, 191–200, doi:10.1029/2000WR900257, 2001.

Jeannin, P. Y. and Marechal, J. C.: Lois de pertes de charge dans les conduits karstiques : base théorique et observations, Bulletin du centre d"Hydrogéologie de Neuchâtel, p. 27p., 1995.

Jukić, D. and Denić-Jukić, V.: Groundwater balance estimation in karst by using a conceptual rainfall–runoff model, Journal of Hydrology, 373, 302–315, doi:10.1016/j.jhydrol.2009.04.035, 2009.

Kiraly, L.: Karstification and groundwater flow, Speleogenesis and Evolution of Karst Aquifers, 2003.

Le Moine, N., Andréassian, V., and Mathevet, T.: Confronting surface- and groundwater balances on the La Rochefoucauld-Touvre karstic system (Charente, France), Water Resour. Res., 44, W03 403, doi:10.1029/2007WR005984, 2008.

Lloyd, J. W. and Heathcote, J. A.: Natural inorganic hydrochemistry in relation to ground water, 1985.

Luhmann, A. J., Covington, M. D., Alexander, S. C., Chai, S. Y., Schwartz, B. F., Groten, J. T., and Jr., E. C. A.: Comparing conservative and nonconservative tracers in karst and using them to estimate flow path geometry, Journal of Hydrology, 448–449, 201 – 211, doi:10.1016/j.jhydrol.2012.04.044, 2012.

Maréchal, J.-C., Ladouche, B., Dörfliger, N., and Lachassagne, P.: Interpretation of pumping tests in a mixed flow karst system, Water Resour. Res., 44, W05 401, doi:10.1029/2007WR006288, 2008.

Martin, J. B. and Dean, R. W.: Exchange of water between conduits and matrix in the Floridan aquifer, Chemical Geology, 179, 145–165, doi:10.1016/S0009-2541(01)00320-5, 2001.

McCuen, R. H.: Hydrologic Analysis and Design, Pearson; 3nd edition, Upper Saddle River, N.J., 2004.

Moussa, R.: Analytical Hayami Solution for the Diffusive Wave Flood Routing Problem with Lateral Inflow, Hydrol. Process., 10, 1209–1227, doi:10.1002/(SICI)1099-1085(199609)10:9<1209::AID-HYP380>3.0.CO;2-2, 1996.

Moussa, R. and Bocquillon, C.: Algorithms for solving the diffusive wave flood routing equation, Hydrol. Process., 10, 105–123, doi:10.1002/(SICI)1099-1085(199601)10:1<105::AID-HYP304>3.0.CO;2-P, 1996a.

Moussa, R. and Bocquillon, C.: Criteria for the choice of flood-routing methods in natural channels, Journal of Hydrology, 186, 1–30, doi:10.1016/S0022-1694(96)03045-4, 1996b.

Moussa, R., Voltz, M., and Andrieux, P.: Effects of the spatial organization of agricultural management on the hydrological behaviour of a farmed catchment during flood events, Hydrological Processes, 16, 393–412, doi:10.1002/hyp.333, 2002.

Mudarra, M. and Andreo, B.: Relative importance of the saturated and the unsaturated zones in the hydrogeological functioning of karst aquifers: The case of Alta Cadena (Southern Spain), Journal of Hydrology, 397, 263 – 280, doi:10.1016/j.jhydrol.2010.12.005, 2011.

Payn, R. A., Gooseff, M. N., McGlynn, B. L., Bencala, K. E., and Wondzell, S. M.: Channel water balance and exchange with subsurface flow along a mountain headwater stream in Montana, United States, Water Resour. Res., 45, W11 427, doi:10.1029/2008WR007644, 2009.

5 Perrin, J., Jeannin, P.-Y., and Cornaton, F.: The role of tributary mixing in chemical variations at a karst spring, Milandre, Switzerland, Journal of Hydrology, 332, 158–173, doi:10.1016/j.jhydrol.2006.06.027, 2007.

Peterson, E. W. and Wicks, C. M.: Assessing the importance of conduit geometry and physical parameters in karst systems using the storm water management model (SWMM), Journal of Hydrology, 329, 294–305, doi:10.1016/j.jhydrol.2006.02.017, 2006.

Reimann, T., Geyer, T., Shoemaker, W. B., Liedl, R., and Sauter, M.: Effects of dynamically variable saturation and matrix-conduit coupling
10 of flow in karst aquifers, Water Resour. Res., 47, W11 503, doi:10.1029/2011WR010446, 2011.

Ruehl, C., Fisher, A. T., Hatch, C., Huertos, M. L., Stemler, G., and Shennan, C.: Differential gauging and tracer tests resolve seepage fluxes in a strongly-losing stream, Journal of Hydrology, 330, 235–248, doi:10.1016/j.jhydrol.2006.03.025, 2006.

Runkel, R. L.: Solution of the Advection-Dispersion Equation: Continuous Load of Finite Duration, Journal of Environmental Engineering, 122, 830–832, doi:10.1061/(ASCE)0733-9372(1996)122:9(830), 1996.

15 Runkel, R. L.: One-dimensional transport with inflow and storage (OTIS): a solute transport model for streams and rivers, Water-Resources Investigations Report, U.S. GEOLOGICAL SURVEY, 1998.

Runkel, R. L. and Chapra, S. C.: An efficient numerical solution of the transient storage equations for solute transport in small streams, Water Resources Research, vol 29, No. 1, pages 211-215, 1993.

Saint-Venant, A. d.: 'Theorie du mouvement non permanent des eaux, avec application aux crues des rivieres et a l'introduction de marees
20 dans leurs lits.", Comptes rendus des seances de l'Academie des Sciences, 36, 147–154, 1871.

Singh, V. P.: Is hydrology kinematic?, Hydrological Processes, 16, 667–716, doi:10.1002/hyp.306, 2002.

Szeftel, P., (Dan) Moore, R., and Weiler, M.: Influence of distributed flow losses and gains on the estimation of transient storage parameters from stream tracer experiments, Journal of Hydrology, 396, 277–291, doi:10.1016/j.jhydrol.2010.11.018, 2011.

Vermot-Desroches, B.: Réalités du changement climatique en Franche-Comté du milieu du XIXe siècle à nos jours, in: Histoire du climat en
25 Franche-Comté du Jurassique à nos jours, éditions du belvédère edn., 2015.

Wang, L., Wu, J. Q., Elliot, W. J., Fiedler, F. R., and Lapin, S.: Linear diffusion-wave channel routing using a discrete Hayami convolution method, Journal of Hydrology, 509, 282–294, doi:10.1016/j.jhydrol.2013.11.046, 2014.

Yu, B., Sombatpanit, S., Rose, C. W., Ciesiolka, C. a. A., and Coughlan, K. J.: Characteristics and Modeling of Runoff Hydrographs for Different Tillage Treatments, Soil Science Society of America Journal, 64, 1763–1770, doi:10.2136/sssaj2000.6451763x, 2000.

Appendix A: Notations

Table A1. Notations

Symbols	Units	Definitions
$*$	$-$	represents the mathematical convolution function
C_M	$[\text{m.s}^{-1}]$	parameter controlling the solute mass flux celerity
C_Q	$[\text{m.s}^{-1}]$	flood wave celerity
D_M	$[\text{m}^2.\text{s}^{-1}]$	parameter controlling the solute mass flux diffusivity
D_Q	$[\text{m}^2.\text{s}^{-1}]$ flood wave diffusivity	
(K_Q, K_M)	$-$	Hayami kernel function for water flow and mass flux modelling, respectively
m	$[\text{kg.s}^{-1}.\text{m}^{-1}]$	lateral mass flux per length unit
M	$[\text{kg.s}^{-1}]$	mass flux
$(M_{I,base}, M_{I,flood}, M_{I,tot})$	$[\text{kg.s}^{-1}]$	upstream base, flood and total mass flux, respectively
$(M_{O,base}, M_{O,flood}, M_{O,tot})$	$[\text{kg.s}^{-1}]$	downstream base, flood and total mass flux, respectively
$(M_{A,base}, M_{A,flood}, M_{A,tot})$	$[\text{kg.s}^{-1}]$	lateral base, flood and total mass flux exchanges, respectively
q	$[\text{m}^2.\text{s}^{-1}]$	lateral flow per length unit
Q	$[\text{m}^3.\text{s}^{-1}]$	discharge
$(Q_{I,base}, Q_{I,flood}, Q_{I,tot})$	$[\text{m}^3.\text{s}^{-1}]$	upstream base, flood and total flow, respectively
$(Q_{O,base}, Q_{O,flood}, Q_{O,tot})$	$[\text{m}^3.\text{s}^{-1}]$	downstream base, flood and total flow, respectively
$(Q_{A,base}, Q_{A,flood}, Q_{A,tot})$	$[\text{m}^3.\text{s}^{-1}]$	lateral base, flood and total flow exchanges, respectively
$(R1, R2)$	$-$	reach 1 (s1 to s2) and reach 2 (s2 to s3), respectively
$(s1, s2, s3)$	$-$	monitoring station 1, 2 and 3, respectively
$(S_{I,base}, S_{I,flood}, S_{I,tot})$	$[\text{g.l}^{-1}]$	upstream solute base, flood and total concentrations, respectively
$(S_{O,base}, S_{O,flood}, S_{O,tot})$	$[\text{g.l}^{-1}]$	downstream solute base, flood and total concentrations, respectively
$(S_{A,base}, S_{A,flood}, S_{A,tot})$	$[\text{g.l}^{-1}]$	lateral solute base, flood and total concentrations, respectively
t	$[\text{s}]$	time
U	$-$	percentage of the unsaturated conduit length along R2
x	$[\text{m}]$	downstream distance
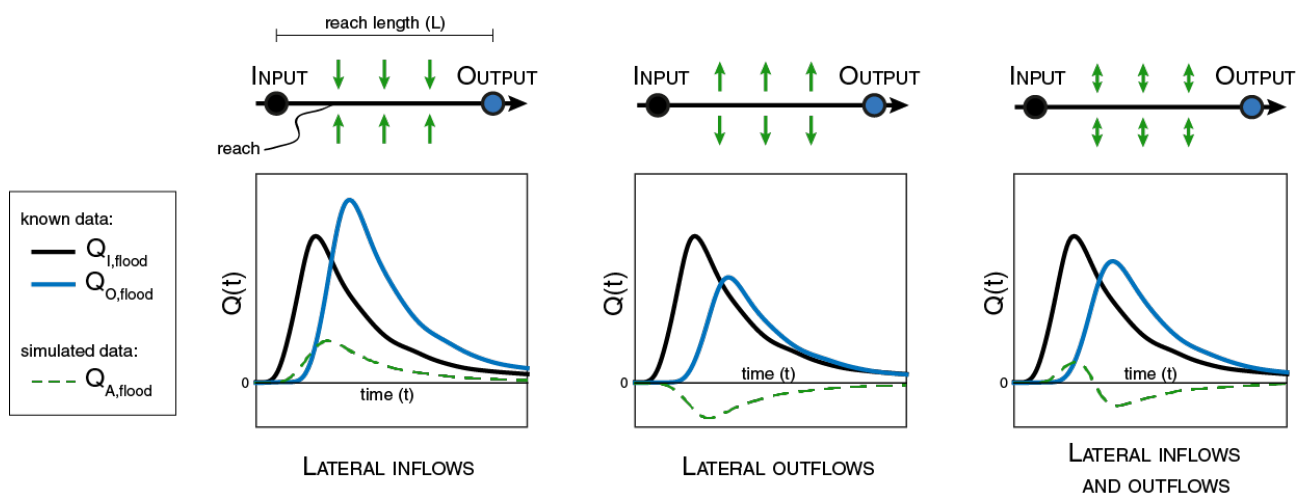
Figure 1. Diffusive wave equation to model lateral flood flow exchanges along a channel reach of length L. The black curve $Q_{I,flood}$ depicts the evolution of the flow rate with time at the beginning of the channel (input), and the blue curve $Q_{O,flood}$ at the end (output). The dashed green curve $Q_{A,flood}$ corresponds to the lateral flow exchanges which are positive for lateral inflows or negative for lateral outflows.
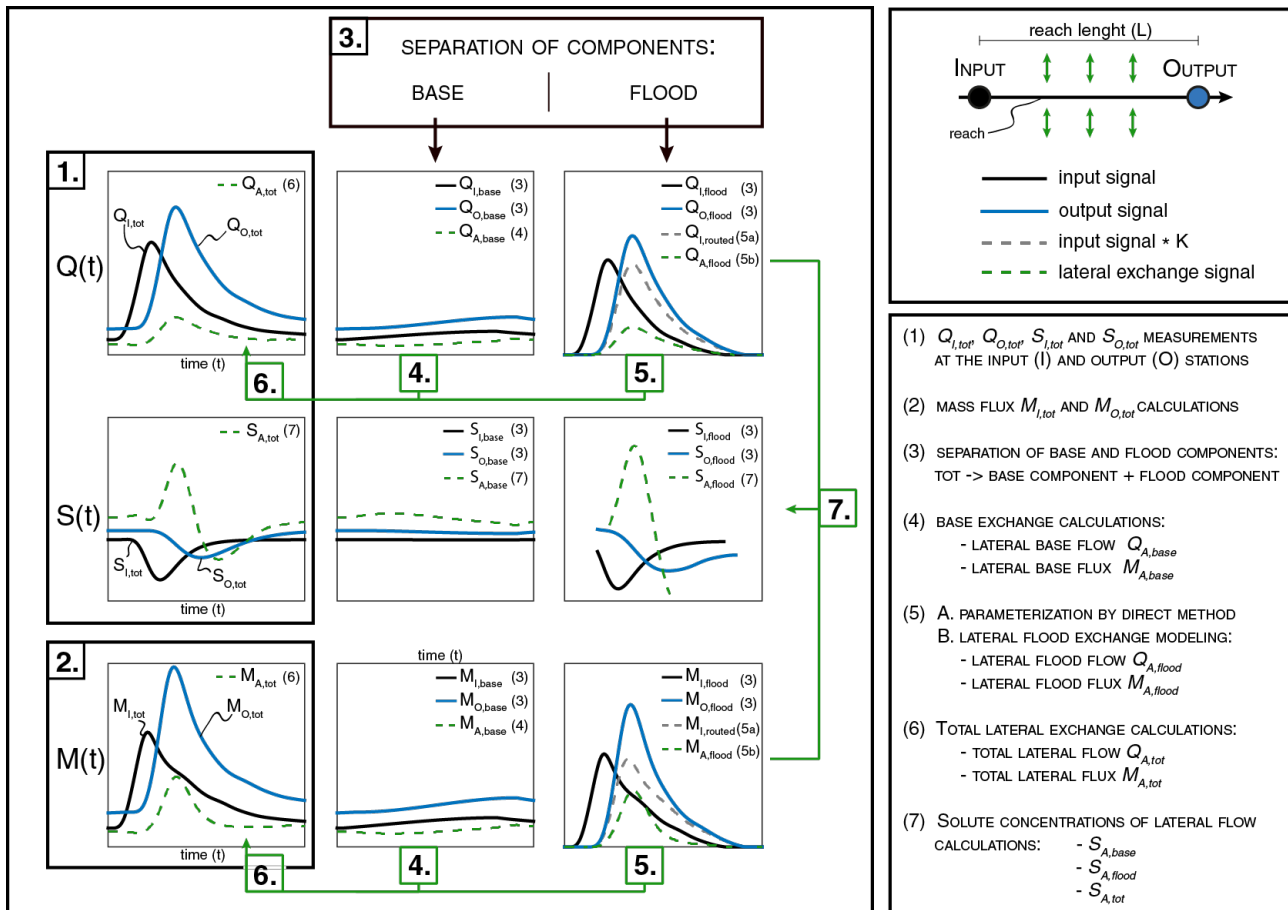
Figure 2. Framework to investigate lateral exchange dynamics of water flows and solute mass fluxes along a channel reach.
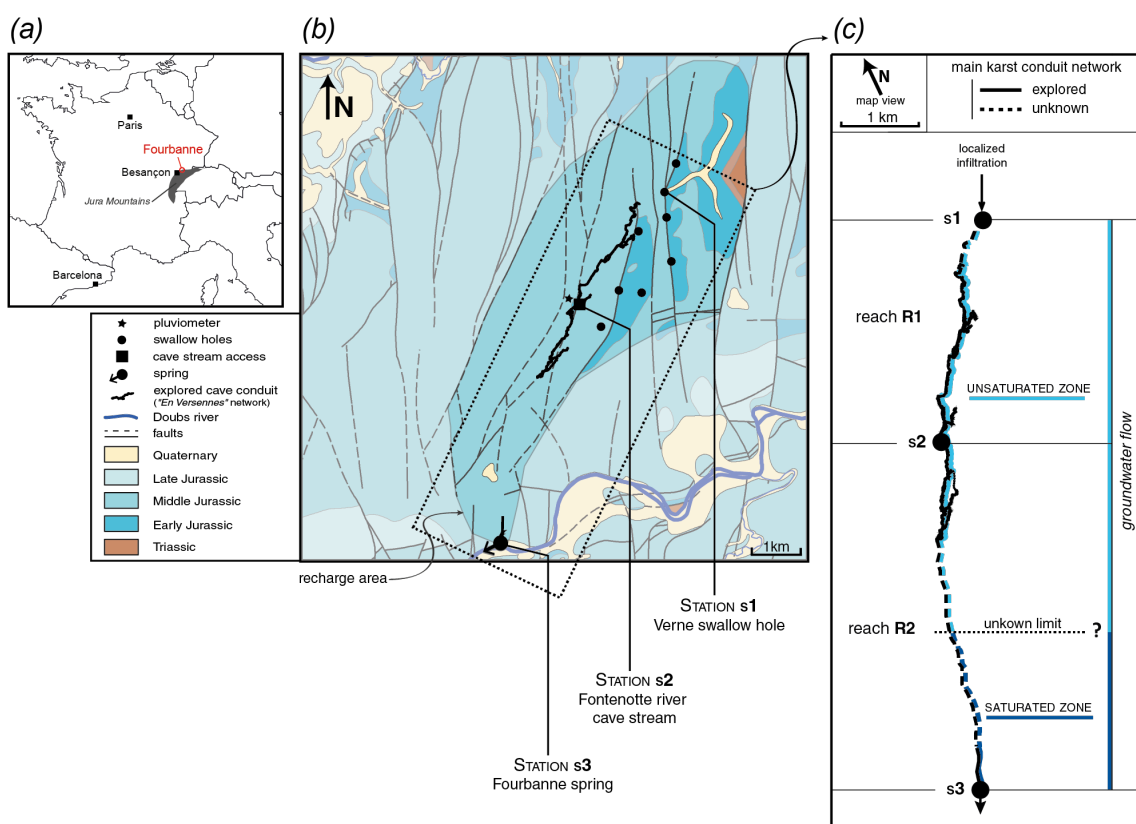
Figure 3. The Fourbanne karst system: (a) geographical localization, (b) hydrogeological map, (c) scheme of the main karst conduit network.

EVENT	1	2	3	4	5	6	7
DATE	27 Feb. 2015	23 Feb. 2015	26 Jan.2015	21 Fev. 2015	11 Fev. 2015	14 Jun. 2015	18 Jun. 2015
TOTAL RAINFALL [mm]	20.8	14.8	9.9	13.5	3.4	46.6	15.2
RAINFALL INTENSITY [mm]	3.0	2.8	1.2	3.2	0.8	17.4	4.7
SPRING BASEFLOW [m³.s⁻¹]	0.80	0.59	0.57	0.52	0.43	0.11	0.10
DISCHARGE [m³.s⁻¹] s1 s2 s3 (spring)							
TDS FLUXES [mg.s⁻¹] s1 s2 s3 (spring)							
HYDROLOGICAL CONDITIONS	← HIGH FLOW				LOW FLOW	EXTREM DRY PERIOD →	
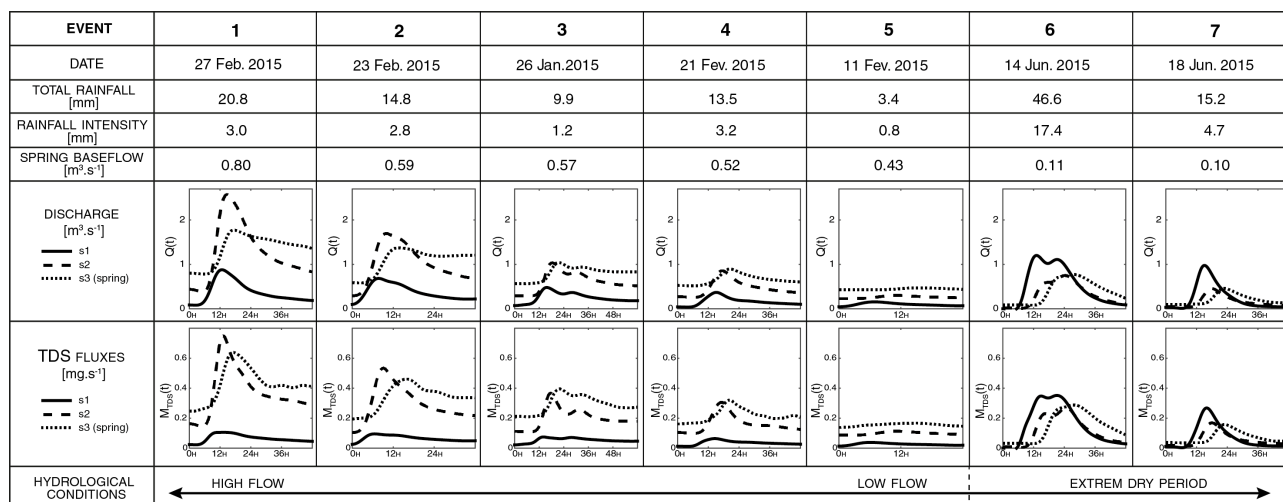
Figure 4. Summary of the flood event selection sorted in function of spring baseflow condition.
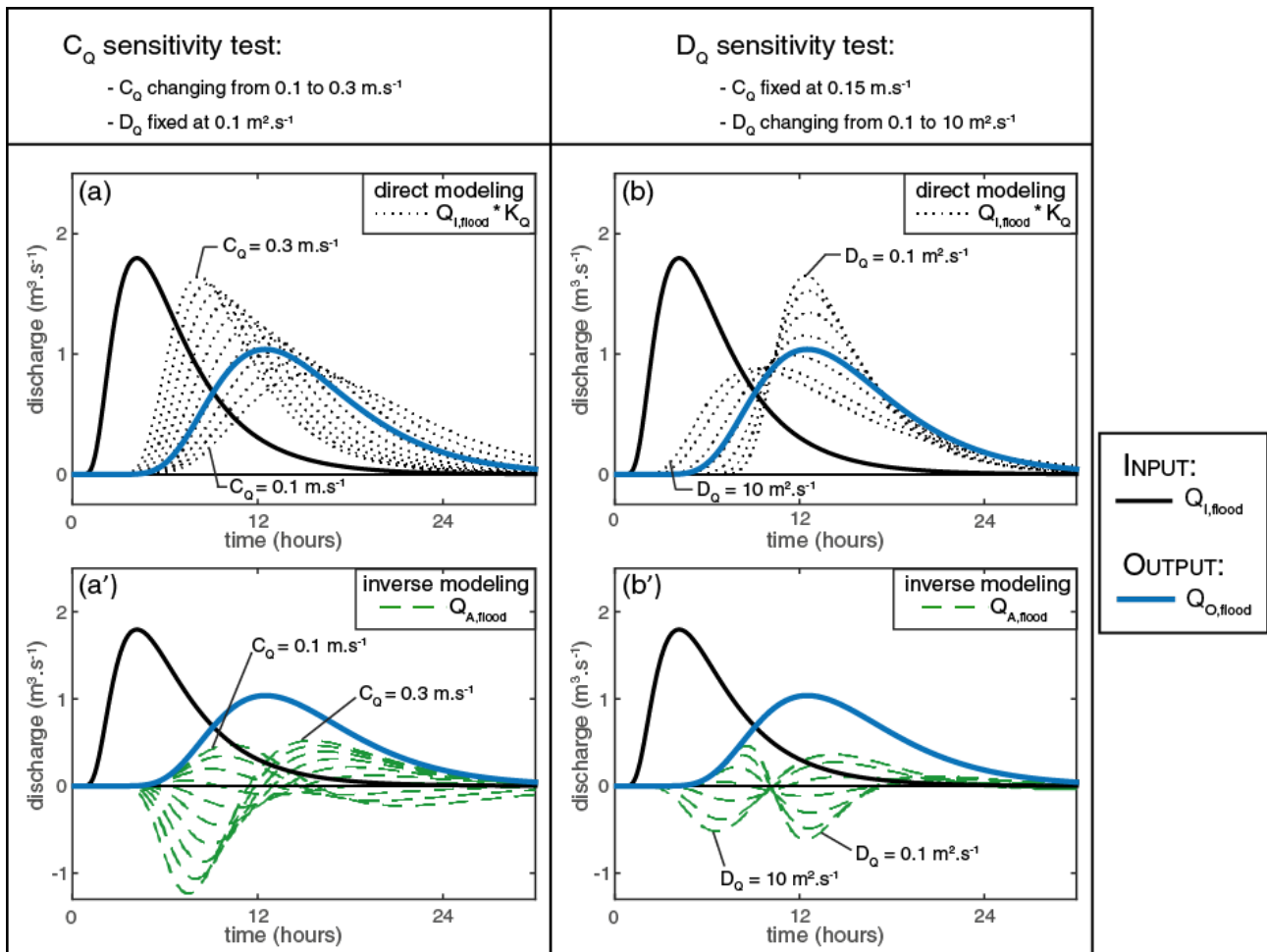
Figure 5. Sensitivity analysis of the model parametrization. Graphs (a-b) illustrate the direct model which simulate the routed input $Q_{I,routed}$ (dashed black lines) without lateral exchange, while graphs (a'-b') illustrate the inverse model which simulate lateral flows $Q_{A,flood}$ (dashed green lines). Graphs (a-a') and (b-b') correspond to sensitivity test of C_Q and D_Q, respectively.
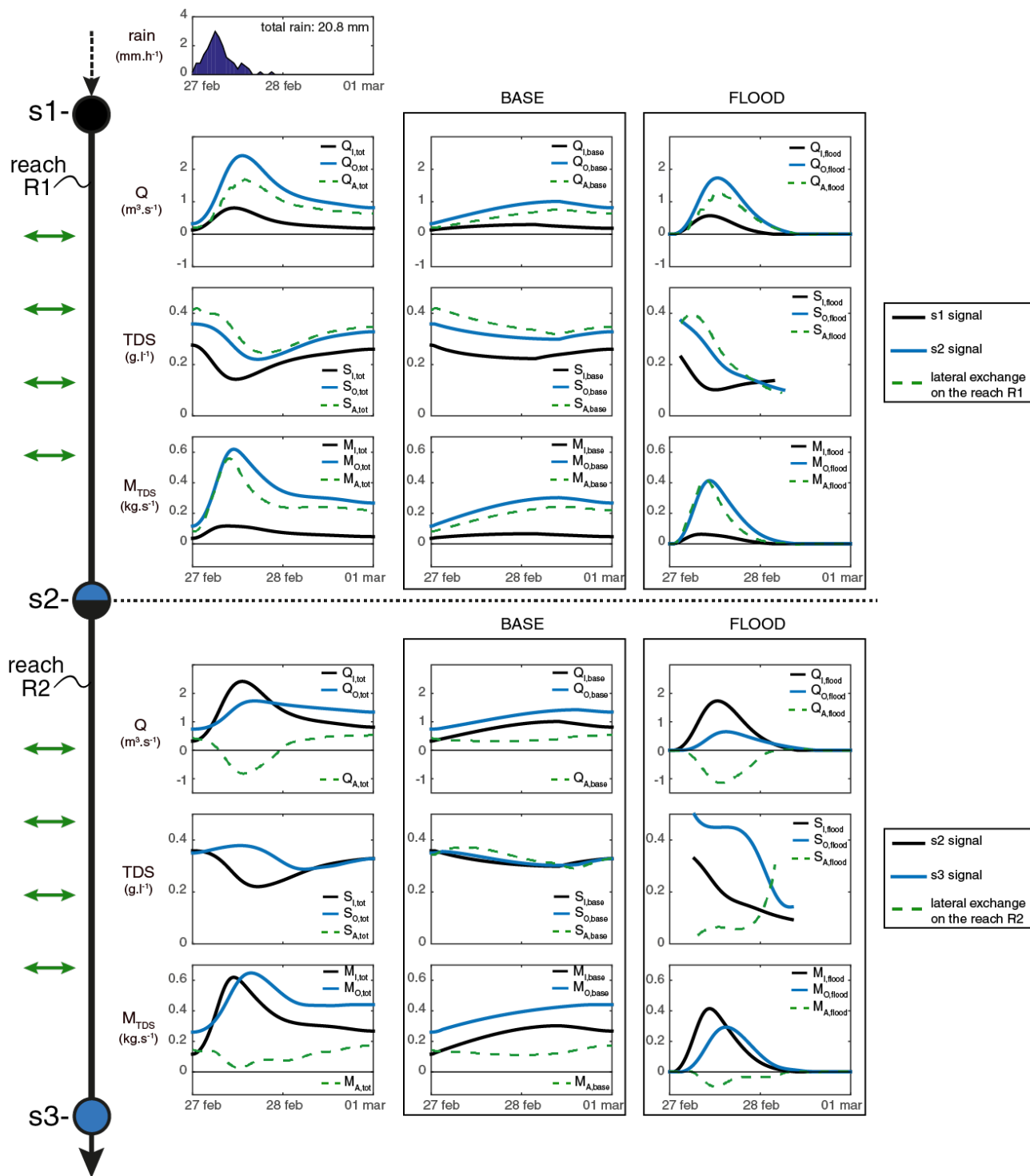
Figure 6. Framework application on the event no. 1 in high flow condition along the 2 reaches R1 (top) and R2 (bottom). Total flow and fluxes, base component and flood component, are represented in the first, second, and third column, respectively.
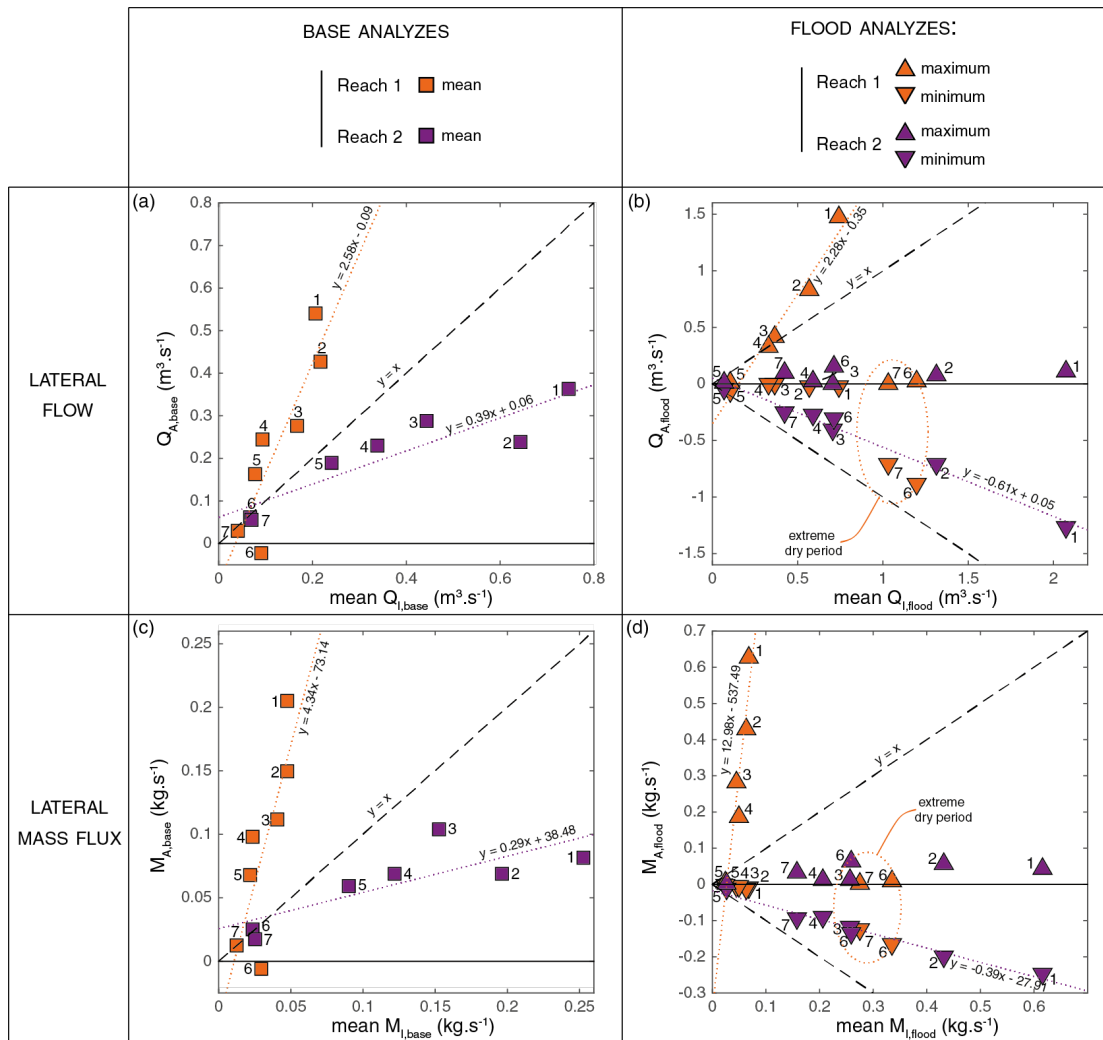
Figure 7. Base and flood analyses of the selected event set. Orange and purple symbols correspond to the lateral exchanges modelling along R1 and R2, respectively. Base analyses is performed on mean values ($\square$) exclusively whereas flood analyses take in account minimum ($\triangledown$) and maximum ($\triangle$) values of the calculated lateral exchanges ($Q_{A,flood}$ & $M_{A,flood}$). Base (a) and flood (b) lateral flow ($Q_{A,base}$ & $Q_{A,flood}$) are compared to the mean base and flood flow input ($Q_{I,base}$ & $Q_{I,flood}$) and base (c) and flood (d) lateral fluxes ($M_{A,base}$ & $M_{A,flood}$) are compared to the mean base and flood fluxes input ($M_{I,base}$ & $M_{I,flood}$).
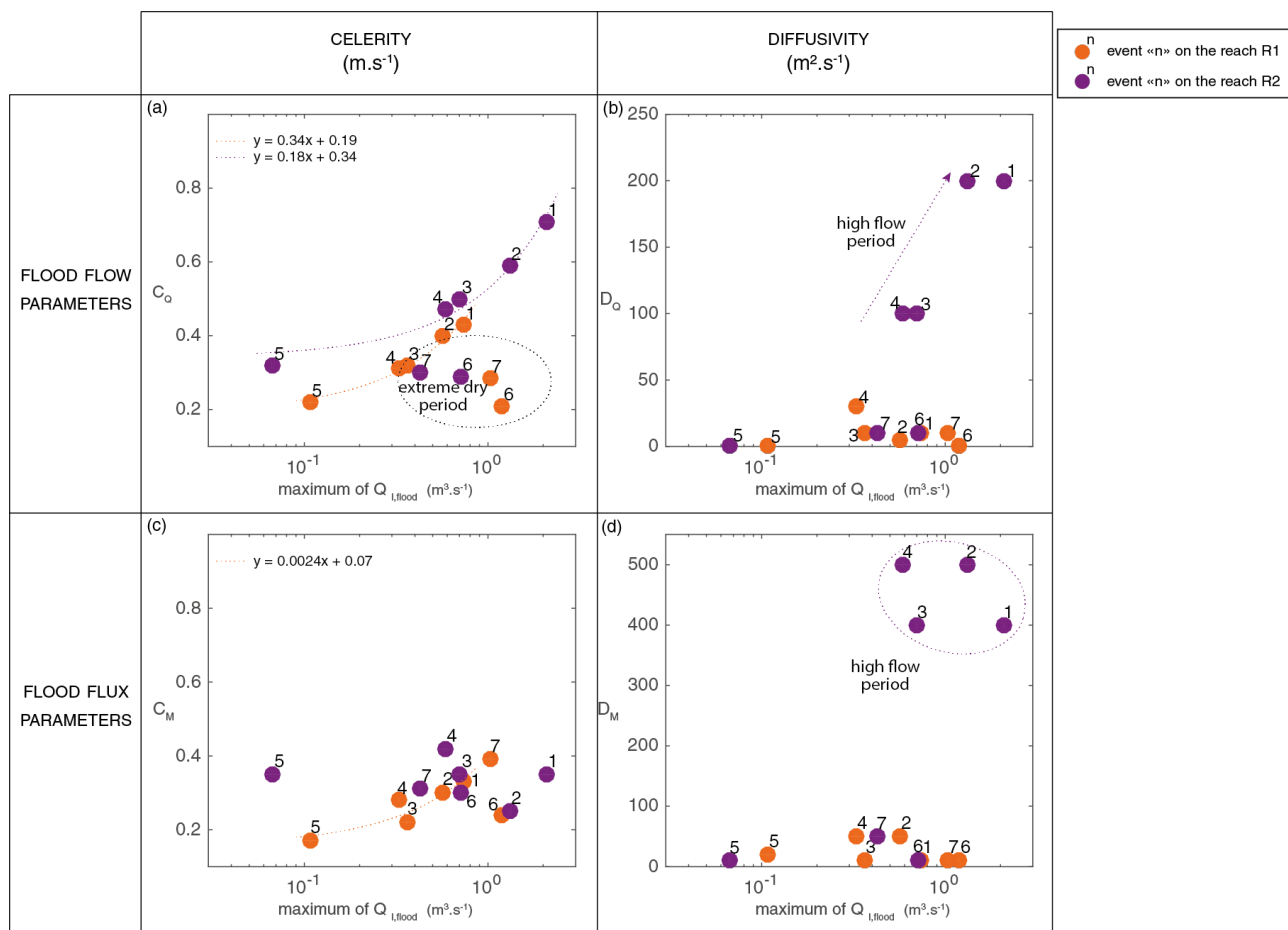
Figure 8. Parametrization analyses of the selected event set. Orange and purple symbols correspond to R1 and R2, respectively. Each parameter of the model is compared with the maximum intensity of the flood flow input signal (logarithmic scale).
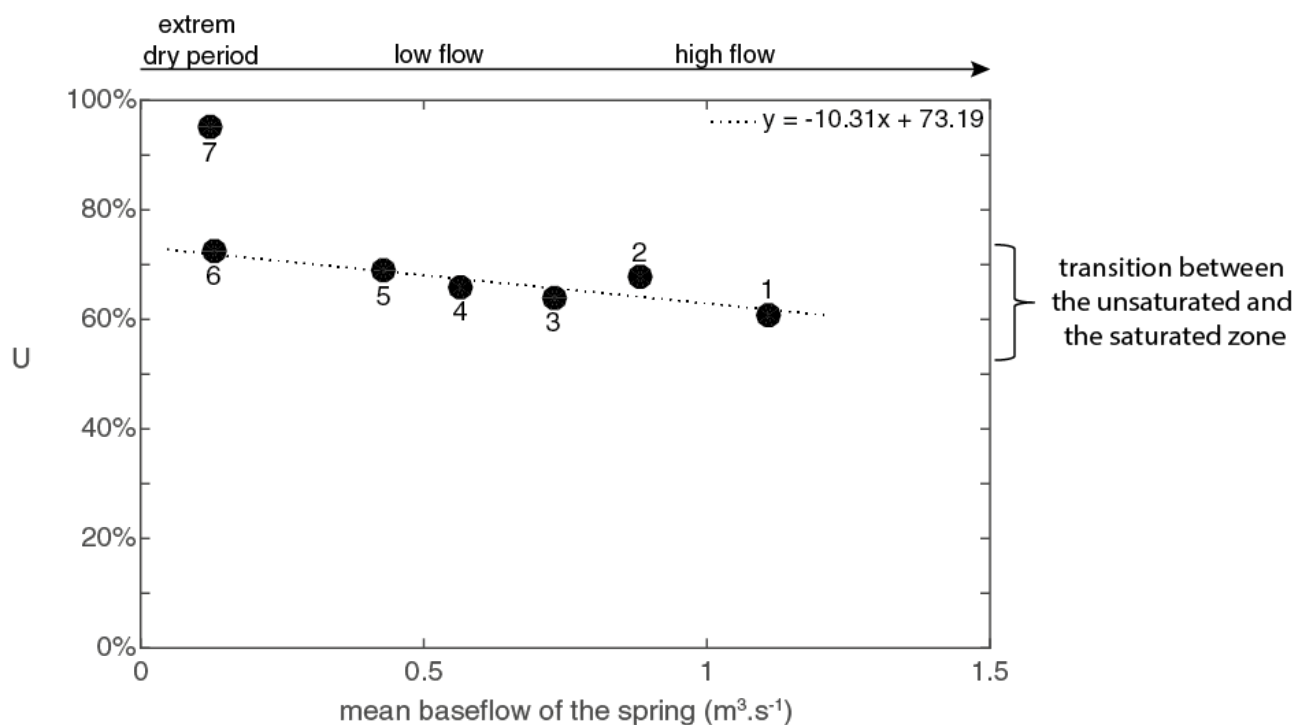
Figure 9. Representation of the limit estimation between unsaturated and saturated conduit along R2 in function of the mean spring base flow. U calculation corresponding to the percentage of conduit length of R2 located within the unsaturated zone.
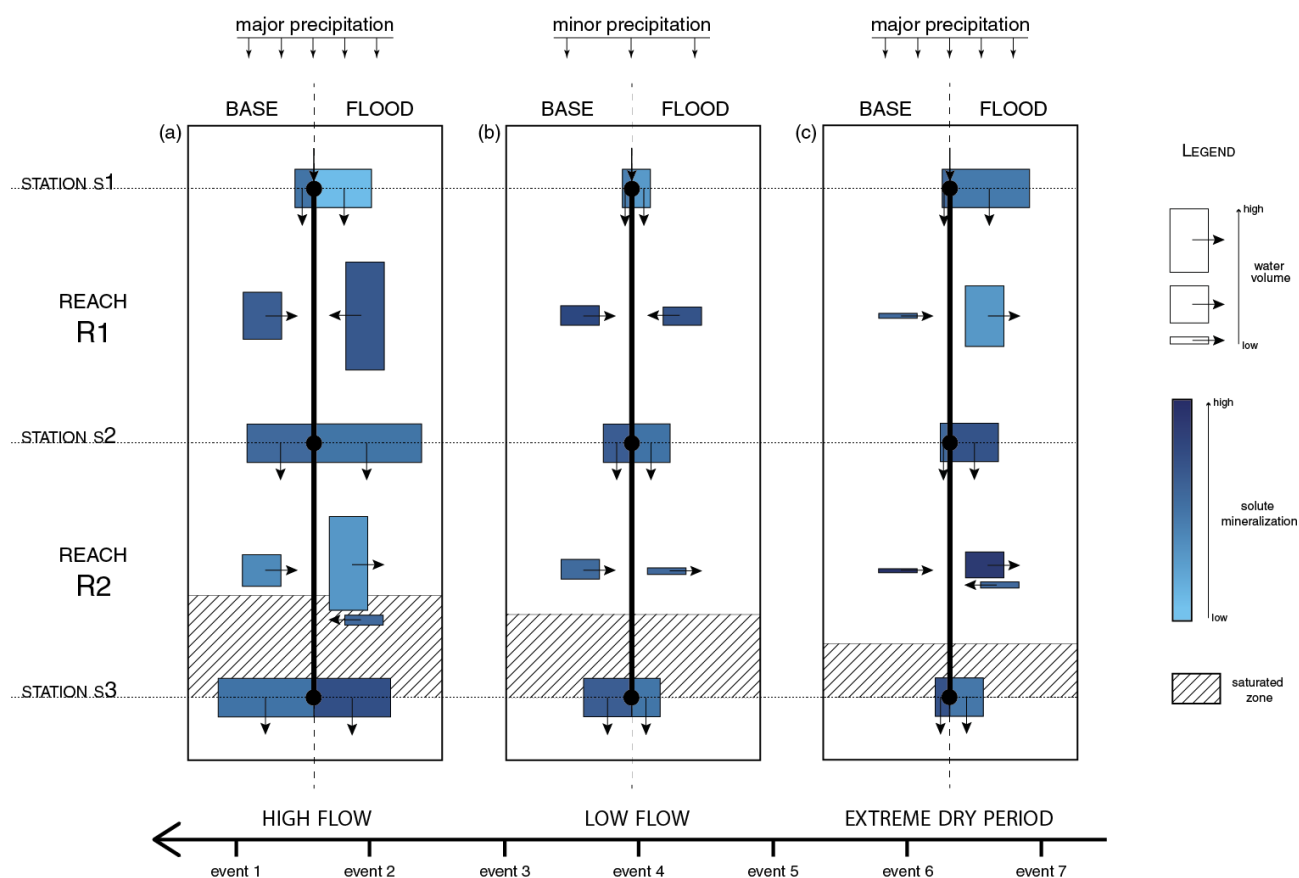
Figure 10. Hydrogeological functioning scheme of the Fourbanne karst aquifer, showing the contributions of lateral exchanges in terms of volume and mineralization for 3 hydrological conditions. For each graph, the representation of the lateral exchanges along the reaches (vertical black line) distinguishes the base component (left size) and the flood component (right size).